Hydrazine network on Cu(111) surface: A Density Functional Theory approach

Saeedeh S. Tafreshi [a], Alberto Roldan [a,b], Nora H. de Leeuw [a,b,*]

[a] Department of Chemistry, University College London, 20 Gordon Street, London WC1H 0AJ, UK
[b] School of Chemistry, Cardiff University, Main Building, Park Place, Cardiff CF10 3AT, UK

A B S T R A C T

We have used first-principles calculations, including a correction for the dispersive forces (DFT-D2), to investigate the arrangement of hydrazine (N_2H_4) molecules upon adsorption on the Cu(111) surface, showing that surface–molecule interactions affect the process most. Our calculations provide insight into the interplay between lateral adsorbate–adsorbate and vertical adsorbate–substrate interactions. We found that the main contributors to the assembly of the hydrazine layers are the binding interactions between the adsorbates and the substrate. The dispersion forces are predominant in both vertical and lateral interactions, whereas hydrogen-bonding is least important and organisation of the N_2H_4 monolayers is therefore primarily due to the long-range interactions. Optimised geometries for several hydrazine conformations were found to be coverage-dependent. The electronic properties such as charge density and density of states have been calculated for different hydrazine coverages, and indicated that no charge transfer occurs between molecules. Scanning tunnelling microscopy images were simulated, where the observed protrusions arise from the trans conformers. We also found that the effect of hydrazine adsorption on the Cu(111) surface energy is negligible and further investigation of other Cu facets is needed to determine the N_2H_4 effect on the nanoparticles' morphology. Finally, we have simulated the temperature programmed desorption of different coverages of hydrazine from the Cu(111) resulting in desorption peaks between 150 and 200 K.

1. Introduction

The assembly of organic molecules on solid surfaces is finding increasing applications in nanoscience, due to the ease of preparation and their power to control surface chemical and physical properties. The driving forces that induce the formation of highly ordered assembled molecular structures on the substrate are the adsorbate–adsorbate and adsorbate–substrate interactions. The molecular orientation during the assembly process may be governed by long-range binding forces such as hydrogen-bonding, dipole–dipole, van der Waals (vdW) and electrostatic interactions which act at a molecular level. Owing to the directional nature of these interactions, especially hydrogen-bonding, they may be used as control tools in the design of assembled monolayers [1]. A fundamental understanding of these interactions will help to better control the structure and properties of these systems [2]. Density Functional Theory (DFT) is a suitable technique to investigate the assembly process at the atomic level and the electronic structures of the systems at different coverages of molecules, as successfully shown on a number of substrates [3–8].

Molecular assembly of adsorbates may also be applied in the synthesis of well-defined nanoparticles for specific applications. Understanding the nanoparticle production process helps us to generate particles with specific sizes, morphologies and desired properties for particular applications. Reverse micelle-based synthesis, for instance, has achieved much in the way of controlling the size and shape of copper nanoparticles, although the underlying processes are still not fully understood. Many factors affect the size and shape of nanoparticles and one important factor is the concentration of the reducing–capping agent, e.g. hydrazine (N_2H_4), which experiment has shown has a strong effect on the nanoparticle morphology [9–15]. Thus, understanding the molecular adsorption of N_2H_4 on the dominant Cu(111) surface at different coverages may help identify measures to control the growth direction and design of copper and other metal nanoparticles.

In this paper we have applied electronic structure calculations based on the Density Functional Theory (DFT), with additional semi-empirical terms to take into account essential dispersion interactions, to investigate the interactions between hydrazine molecules. We have investigated the systems with different concentrations of hydrazine, forming a network layer at the molecular level, to provide insight into the interplay between lateral adsorbate–adsorbate and vertical

* Corresponding author. Tel.: +44 2920870658.
E-mail address: DeLeeuwN@cardiff.ac.uk (N.H. de Leeuw).

adsorbate–substrate interactions, and to deduce the effect of the concentration of hydrazine on the copper crystal shape. The application of a full monolayer allows us to mimic the hydrazine assembly and understand the intermolecular interactions. We have also modelled scanning tunnelling microscopy (STM) images for future comparison with experiment.

2. Computational methods

In this study we have employed the Vienna Ab-initio Simulation Package (VASP) [16,17], which allows calculations based on the Density Functional Theory (DFT) [16–19] using pseudopotentials and plane-wave basis sets. The Perdew, Burke and Ernzerhof (PBE) [20] form of the GGA pseudopotentials [21,22] is used here for calculations within the general gradient approximation, to carry out our total energy calculations and perform geometry optimisations by minimizing the forces and stress tensor on the systems. Only the valence electrons were treated explicitly and their interactions with the ionic cores were described by the Projector Augmented-Wave (PAW) method [22]. The cut-off energy for the expansion of the plane-wave basis sets was set at 600 eV, which gave bulk energies converged to within 0.001 eV/atom. To improve the description of the long-range interactions, we have employed the DFT-D2 [23,24] method of Grimme as implemented in VASP, which has been shown to make important contributions to the surface–molecule interactions [3,25–27]. In this approach the total energy is calculated as a function of the dispersion coefficient for each atom pair, a global scaling factor that depends only on the exchange–correlation functional used, which is 0.75 for the PBE functional, and a damping function to avoid near singularities for small distances. The integration of the Brillouin zone was done using the Monkhorst–Pack [28] $11 \times 11 \times 11$ and $3 \times 3 \times 1$ k-point grids for the bulk and surface simulations, respectively.

Following our previous work [25,26], we have used a slab model of four atomic layers, in which the three uppermost layers were free to relax during the optimization, while the bottom layer was kept frozen at the optimised bulk positions. This set-up, where one side of the slab is kept fixed, ensures the explicit geometry optimisation of a realistic number of surface layers, while still retaining a reasonably sized slab which made it feasible to investigate a large number of initial adsorption geometries. To evaluate the model, structural relaxations of the clean Cu(111) surfaces were performed as a measure of the accuracy of the surface structure. They are calculated as the percentage relaxations of the atomic layers using Eq. (1):

$$\Delta d_{ij}\% = \left[\left(d_{ij} - d_{bulk}/d_{bulk} \right) \right] \times 100 \tag{1}$$

where d_{ij} is the interlayer distance in the relaxed surface and d_{bulk} is the bulk layer spacing, which is given by the spacing of the fixed layers in the slab. The results for a 4-layer slab with different numbers of relaxed layers are summarised in Table 1, where minus signs correspond to contraction. We note a contraction (-0.12%) in the first interlayer relaxation of the Cu(111) surface with three relaxed layers, in good agreement with experiment. Furthermore, the second interlayer exhibits an even larger contraction (-0.40%), while the interlayer spacing d_{34} (-0.04%) remains almost unchanged.

We have also calculated the relaxed surface energies for the clean Cu(111) with different numbers of relaxed layers, where the unrelaxed surface energy (γ_u) is calculated as follows, Eq. (2):

$$\gamma_u = \frac{E_{slab,u} - nE_{bulk}}{2A}. \tag{2}$$

$E_{slab,u}$ is the energy of the unrelaxed slab, E_{bulk} is the energy of the primitive cell, n is the number of atoms in the slab compared with the ones in the bulk and A is the surface area of one side of the slab. We have then calculated the relaxed surface energy (γ_r) using Eq. (3); where $E_{slab,r}$ is the energy of the relaxed slab with one side fixed in the optimised bulk geometry.

$$\gamma_r = \frac{E_{slab,r} - nE_{bulk}}{A} - \gamma_u \tag{3}$$

Table 1 presents the relaxed surface energies for a 4-layer slab with different numbers of relaxed layers, which shows that the surface energies converge very well with respect to the number of relaxed layers for the Cu(111) surface.

The slab used is a 3×3 supercell from the full unit cell, $p(6 \times 6)$, containing 36 atoms per layer (144 Cu atoms/unit cell) and exposing an area of 198.8 Å^2, which enables us to investigate a realistic hydrazine network. A vacuum of 20 Å was included between the slabs to avoid perpendicular interactions between images. We have also employed a perpendicular dipole correction to enhance energy convergence of the adsorbed systems. The geometry of the hydrazine molecule was optimised in the gas phase using a cubic box of $20 \times 20 \times 20$ Å^3, where the relaxed gauche conformer was found to be the most stable structure, being lower in energy by 0.13 eV relative to the trans and by 0.36 eV relative to the eclipsed conformation.

We started building an overlayer of hydrazine molecules from a single hydrazine on the Cu(111), as investigated previously [25], and increasing to two, three, four, five, six and nine molecules per cell, resulting in a wide range of coverages: from 0.50 to 4.53 molecules/nm^2. We carried out a relaxation of the geometry after each addition.

The adsorption energy (E_{ads}) per molecule was calculated as the difference between the total energy of the optimised substrate–adsorbate system ($E_{slab+nmol}$) and the sum of the energy of the relaxed clean surface (E_{slab}) and n times the energy of an isolated N$_2$H$_4$ (E_{mol}) in the gauche conformation, which is the most stable hydrazine conformer in the gas phase; n is the number of hydrazine molecules, Eq. (4):

$$E_{ads} = \left[E_{slab+nmol} - (E_{slab} + n \cdot E_{mol}) \right]/n. \tag{4}$$

The binding and cohesion energies per molecule have also been calculated to discuss the interplay between transversal (E_{bind}) and lateral interactions (E_{cohe}) [32], which are defined as

$$E_{bind} = \left[E_{slab+nmol} - \left(E^*_{slab} + E_{nmol} \right) \right]/n \tag{5}$$

$$E_{cohe} = [E_{nmol} - nE_{mol}]/n \tag{6}$$

where, E_{nmol} is the energy of the hydrazine network in the vacuum and E^*_{slab} is the energy of the copper surface, both with the same geometry as found in the adsorbate–substrate calculation (denoted by the asterisk). Within this definition, negative E_{ads}, E_{bind} and E_{cohe} values mean a

Table 1
The relaxed surface energies γ and percentage interlayer relaxation of clean Cu(111) slabs with different numbers of relaxed layers.

	Bulk	1 relaxed layer	2 relaxed layers	3 relaxed layers	Exp
γ (J/m^2)	1.9714	1.9712	1.9696	1.9695	2.02 [29]
Δd_{12} (%)	–	−0.08	−0.08	−0.12	−0.7 ± 0.5 [30], −0.3 ± 1.0 [31]
Δd_{23} (%)	–	–	−0.44	−0.40	–
Δd_{34} (%)	–	–	–	−0.04	–

release of energy during the adsorption process, but when we compare in the discussion of the results any energies adsorbed or released, we comment only on their magnitudes. The Bader population analysis as implemented by the Henkelman algorithm [33] is also used to clarify the nature of the binding between molecules and the surface.

The scanning tunnelling microscopy (STM) images were simulated using the Tersoff–Hamann formalism [34], in which tunnelling currents are proportional to the local density of states (LDOS) of the surface over a range that corresponds from the Fermi energy (E_F) to the bias. We integrated our DFT-based partial charge density from -1.5 eV to E_F using Hive [35]. An STM at constant current mode follows a surface of constant current, which translates into a surface of constant integrated LDOS $\rho(x, y, z) = \rho_c$ as a function of x, y and mapping z on a grayscale.

3. Results and discussion

An isolated hydrazine molecule prefers to adsorb parallel to Cu(111) in a gauche conformation, but rotated towards the eclipsed conformation, interacting through both nitrogen atoms with Cu–N distances of 2.16 and 2.17 Å, as shown in Table 2. This structure with the calculated adsorption energy of -0.85 eV/N_2H_4 and a long-range interaction energy contribution of -0.61 eV/N_2H_4 is shown in Fig. 1 [25]. As we have shown in our previous papers [25,26], the dispersion correction enhances the hydrazine adsorption on the Cu(111) surface and increases the adsorption energy, while it changes the preferred orientation of the molecule from the atop geometry obtained by pure DFT [36] to a bridging adsorption configuration by using dispersion-corrected DFT-D2.

We have modelled several hydrazine configurations to produce the hydrazine assembly. We started from two molecules and identified the lowest-energy configuration, followed by a further increase in the coverage through the addition of another molecule onto the surface and exploration of the different orientations under the new coverage. The hydrazine network was grown in this way until full monolayer coverage was obtained. The lowest-energy structures are shown in Figs. 1–3, whereas less stable configurations are provided in the Supplementary Information. We have reported the adsorption, binding, and cohesion energies for each system, as well as the dispersion contributions to the energies, in Table 3 and the geometric details in Table 2.

3.1. Adsorption structures of hydrazine molecules on Cu(111)

First, we investigated the relative orientation between two molecules in the supercell, as shown in Fig. 1. We positioned different hydrazine conformers, including gauche, trans and eclipsed conformers, onto the surface, providing several choices for pairing of the N_2H_4 molecules. We found three low-energy configurations with only small differences in the adsorption energies, $\Delta E_{ads}^{2(A)-2(B)} = -0.06$ eV and $\Delta E_{ads}^{2(A)-2(C)} = -0.03$ eV, as shown in Table 3. Structure 2(A) has one hydrazine in the gauche and its neighbouring molecule in the trans conformation. In structure 2(B) one hydrazine is in the gauche

conformation, adsorbing through one N atop a Cu atom, while the other molecule rotates towards the eclipsed conformation, thereby enabling the molecule to bridge through both N atoms to the surface. In the third structure, 2(C), both molecules are in the gauche conformation and, like structure 2(A), they adsorb on the surface through one N atom.

Configuration 2(A) binds most strongly, due to the higher contribution of the dispersion interaction (Table 3). Although there is negligible difference in charge transfer (CT) from the hydrazine clusters to the surface, $\Delta(CT)^{2(A)-2(B)} = -0.02$ e$^-$ and $\Delta(CT)^{2(A)-2(C)} = +0.03$ e$^-$, the molecules in structure 2(A) are closer to the surface. The structure of the trans conformer makes it feasible to form H-bonds with nitrogen atoms of the neighbouring gauche conformer and enables molecules to interact by lateral interactions. Structure 2(A) is stabilised by the dispersive forces which contribute half of the adsorption energy. Since in structure 2(B) the hydrazine assembly has bound covalently to the surface through three bonds, compared to two bonds in 2(A) and 2(C), it leads to more charge transfer ($+0.19$ e$^-$) and a larger binding energy to the surface (-1.19 eV), the largest of the calculated structures (Table 3). However, the longer distance and weaker interaction between the molecules result in a smaller adsorption energy. Owing to the closer distance between the molecules in structure 2(C), this has the highest cohesion energy, although the repulsion between the hydrogens of the two gauche conformers decreases the adsorption energy.

We next increased the coverage by adding a third molecule to the previous three configurations, where the most stable networks formed are indicated as 3(A), 3(B) and 3(C) in Fig. 2. In the 3(A) network, which is grown from the optimised 2(A) geometry, the adsorption energy decreases to $E_{ads} = -1.10$ eV through the addition of another gauche hydrazine, which forms an H-bond between one of the nitrogen atoms and one of the H atoms of the trans conformer. The charge transfer from the molecules to the surfaces is also the largest of these three configurations, making this the most stable structure at this coverage.

Configuration 3(B) grown from 2(B), decreases the adsorption energy to -1.03 eV compared to 3(A), $\Delta E_{ads}^{3(A)-3(B)} = -0.07$ eV. In this case, one of the hydrazine molecules bridges through both nitrogen atoms to the surface, whereas the others, in gauche conformation, bind only by one nitrogen to the copper atoms, allowing the formation of hydrogen bonds through their N to hydrogen atoms of the 'bridging' hydrazine in the middle. Structure 3(C) grows from 2(C), with all hydrazine molecules in gauche conformation and interacting through only one nitrogen atom to the surface, releasing a smaller adsorption energy of $E_{ads} = -1.01$ eV, i.e. -0.09 eV less favourable than configuration 3(A). The energy difference is related to the smaller charge transfer from the molecules to the surface (shown in Table 2). The 3(C) has the highest cohesion energy among the calculated configurations, $E_{cohe} = -0.10$ eV, which is due to the short distance between the molecules and therefore stronger H-bonds.

Based on the lowest-energy structure found for the $[N_2H_4]_n$ assembly by three molecules (n = 3), we increased the coverage by adding one and two extra molecules to this network. Fig. 3 shows the lowest-energy assemblies of $[N_2H_4]_n$ clusters (n = 4, 5), with three and four H-bonds respectively. The calculated energies for these structures, (Table 3), show that the clusters are energetically degenerate ($\Delta E_{ads}^{4-5} = -0.01$ eV), indicating that the extra H-bond in the structure does not contribute much to the stability of the structure and confirming that the hydrazine assembly is mostly due to dispersion forces.

The lowest-energy $[N_2H_4]_6$ assembly on the surface is shown in Fig. 3 with an adsorption energy of $E_{ads} = -1.01$ eV, the same adsorption energy than 3(C). It is grown from 3(A) and consists of two trans structures in the centre, neighboured by four gauche conformers, with all the molecules binding to the surface through one N atom. Although there are four H atoms oriented towards the N of a neighbouring molecule, the calculated cohesion energy ($E_{cohe} = -0.05$ eV) varies little and is of a similar magnitude compared to the other hydrazine assemblies with

Table 2
Distances (d) and charge transfer (CT) between the surface and the cluster on the most-stable structures with one, two and three N_2H_4 molecules on the Cu(111). The distances between the interacting Cu atoms and the N atoms of each N_2H_4 molecule are reported.

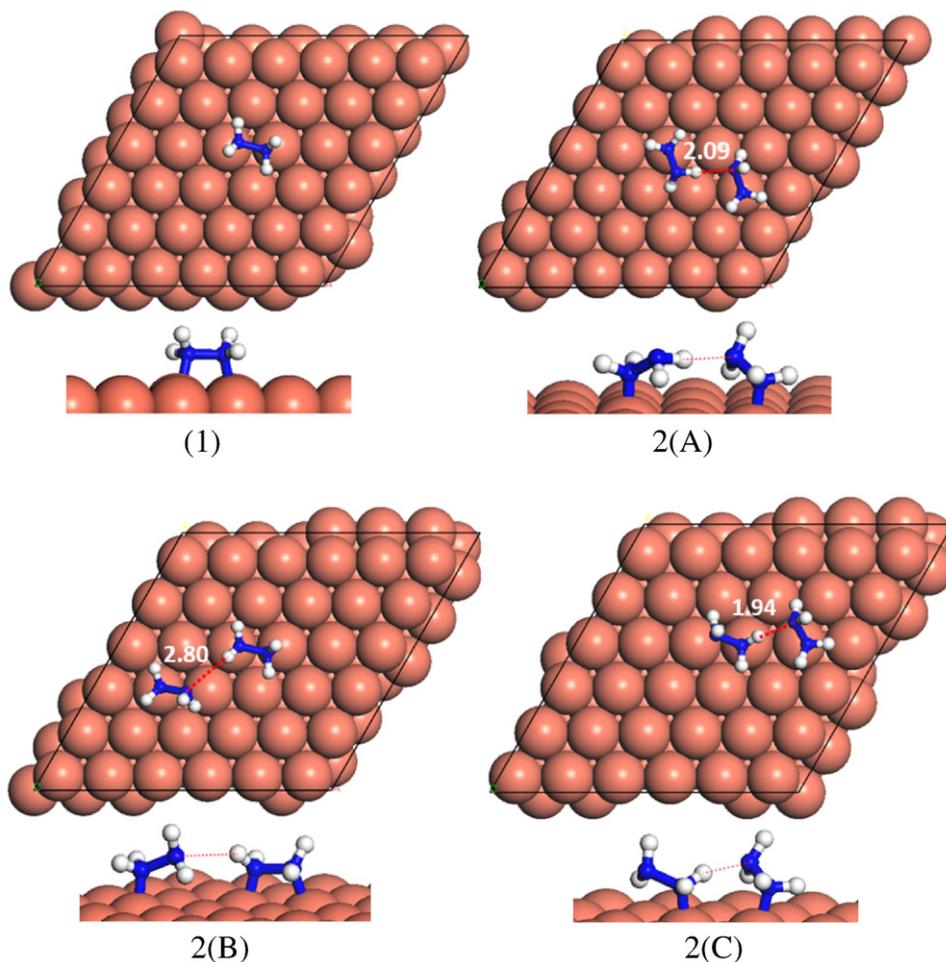| No. hydrazines	d_{N-Cu} (Å)	d_{N-Cu} (Å)	d_{N-Cu} (Å)	$d_{(H-bond)}$ (Å)	CT (e$^-$)
1	2.16	2.17	–	–	+0.14
2(A)	2.08	2.12	–	2.09	+0.17
2(B)	2.13	2.11, 2.25	–	2.80	+0.19
2(C)	2.10	2.14	–	1.94	+0.14
3(A)	2.14	2.07	2.12	2.33, 2.14	+0.23
3(B)	2.12	2.16, 2.16	2.12	3.34, 3.32	+0.21
3(C)	2.10	2.12	2.14	2.30, 1.94	+0.19

Fig. 1. Top and side views of the lowest-energy N_2H_4 adsorption configurations of (1), single N_2H_4 molecule adsorption, and 2(A), 2(B) and 2(C) configurations for two molecules on the Cu(111) surface. The hydrogen-bond distances are indicated and labelled in Å (N = blue, H = white, Cu = orange).

fewer hydrogen-bonds, which is due to the relatively long and weak hydrogen-bonds between molecules.

By adding three more hydrazine molecules and increasing the coverage to nine molecules (4.53 molecules/nm²), aimed at attaining full coverage, we found the lowest-energy configuration with an adsorption energy of $E_{ads} = -0.95$ eV/N_2H_4 and dispersion contribution of $E_{ads}^{vdW} = -0.58$ eV/N_2H_4, represented in Fig. 3. Together with

$E_{cohe} = -0.07$ eV/N_2H_4 and $E_{bind} = -0.92$ eV/N_2H_4, these results indicate that the binding of the N_2H_4 molecules to the Cu surface is the main contributor to the stabilisation of the hydrazine network, owing to the covalent character of the interaction of all molecules with the surface [25,26]. Dispersion forces make up almost half of the adsorption and binding energies, showing that the dispersive forces are also essential in the description of the hydrazine organisation. The
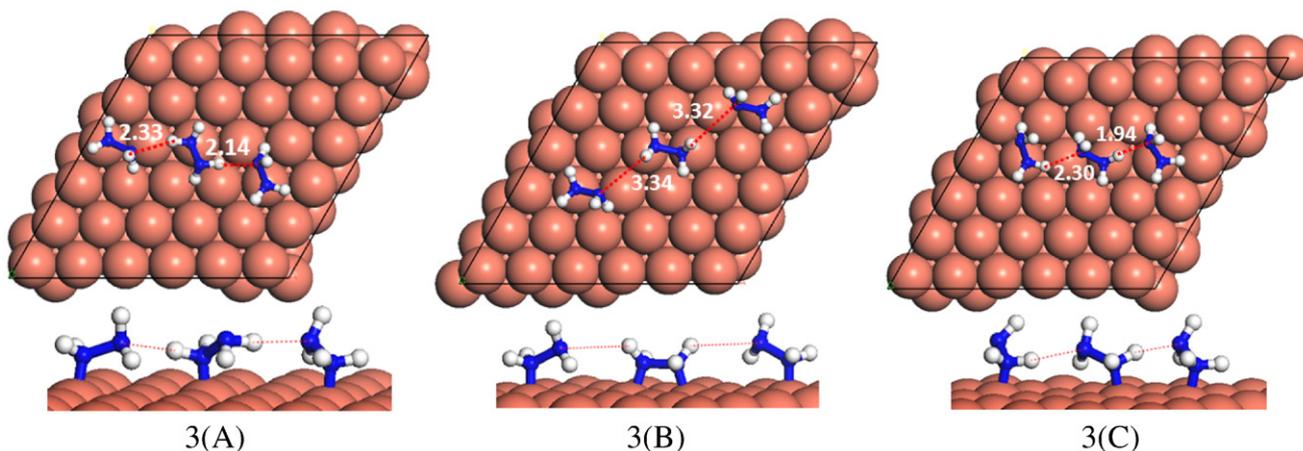

Fig. 2. Assembly of hydrazine configurations 3(A), 3(B) and 3(C) for three molecules on the Cu(111) surface. The hydrogen-bond distances are indicated and labelled in Å (N = blue, H = white, Cu = orange).
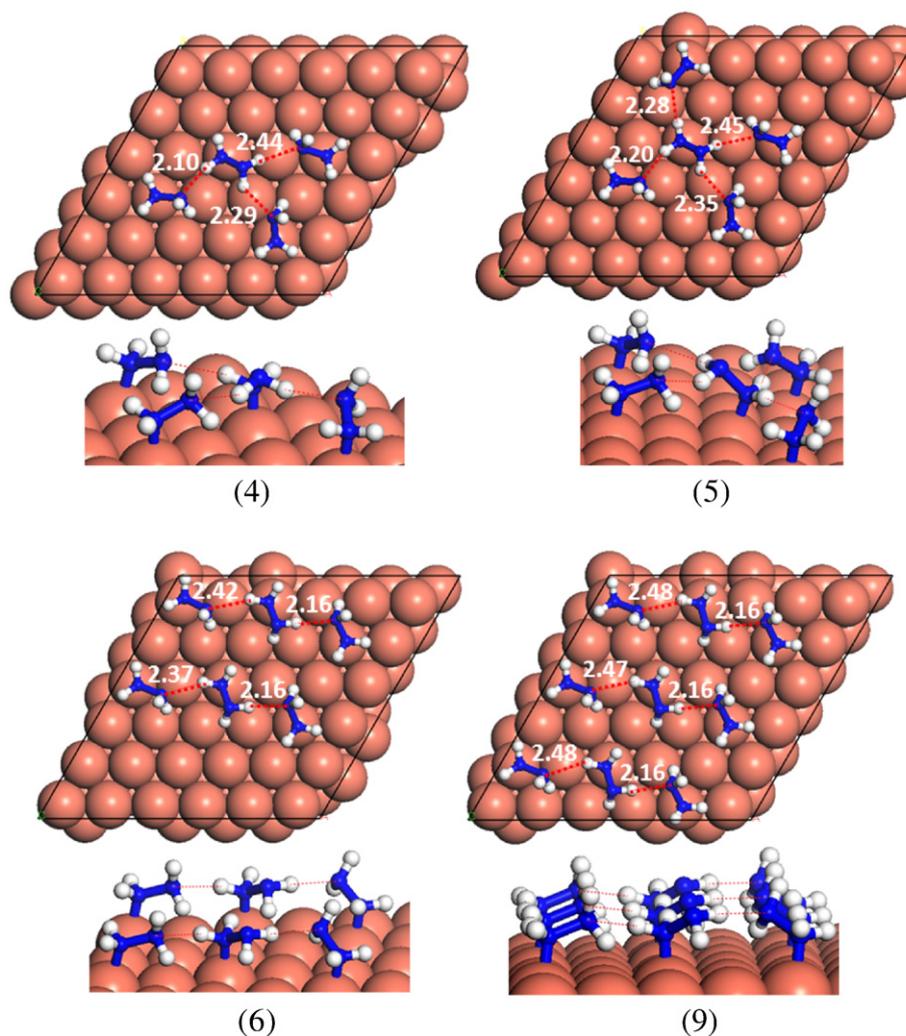
Fig. 3. Self-assembly of hydrazine for four, five, six and nine molecules on the Cu(111) surface. The hydrogen-bond distances are indicated and labelled in Å (N = blue, H = white, Cu = orange).

high contribution of dispersion forces to the small cohesion energies indicate that van der Waals forces are the main interaction between molecules, whereas hydrogen-bonding is only a weak factor in the formation of the hydrazine assemblies, because of the relatively long distances between molecules.

3.2. Electronic structure characterization

We have calculated the charge density differences for hydrazine on the Cu(111) surfaces by subtracting the individual electron densities of the molecular cluster and the surface, both calculated in the geometry of the combined system, from the density of the total system, see Fig. 4. Yellow and blue regions correspond to positive and negative electronic charge modifications, respectively, between the Cu substrate and molecules.

The charge density difference has been calculated for two different coverages of hydrazine on the Cu(111), i.e. with 5 and 9 molecules. The electronic density rearrangement takes place individually, with negligible polarization of the molecular electron clouds, which is quite similar to the single molecule adsorption. This electronic behaviour matches the energetics, showing that the molecule–surface interactions (binding energy) contribute most to the hydrazine assembly.

Table 3
Adsorption (E_{ads}), binding (E_{bind}) and cohesion (E_{cohe}) energies. Long-range interaction energy contributions to these energies are also reported with vdW superscript.

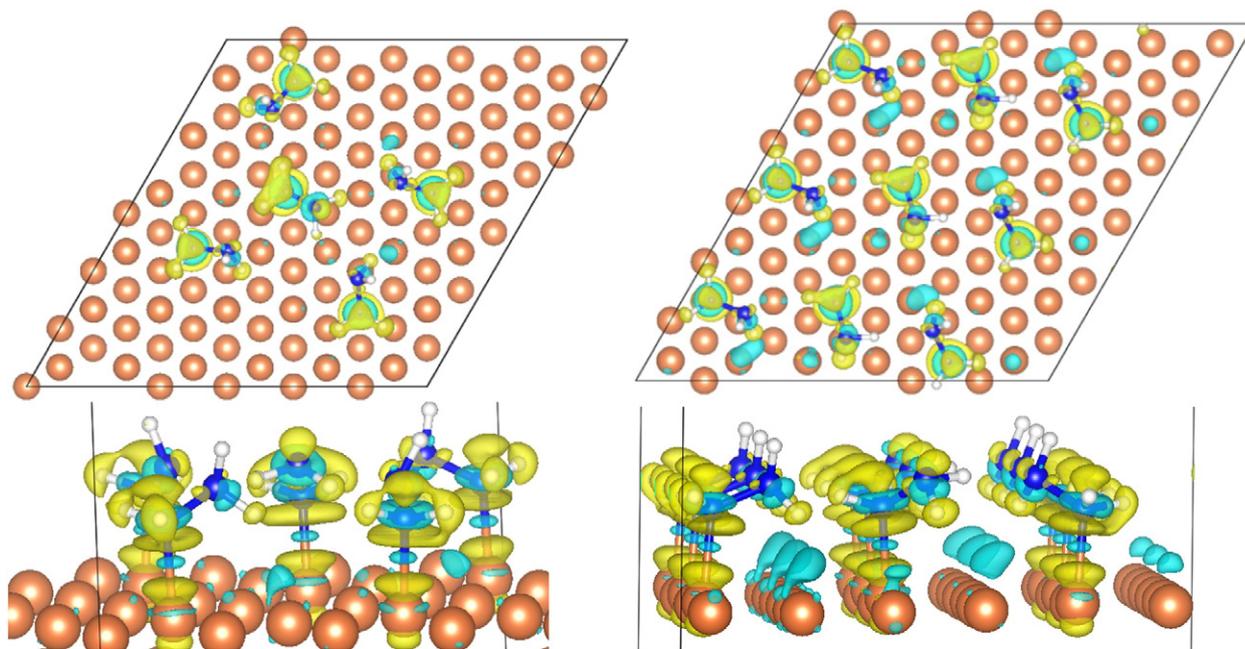| No. hydrazine (types)	E_{ads} (eV/N$_2$H$_4$)	E_{ads}^{vdW} (eV/N$_2$H$_4$)	E_{bind} (eV/N$_2$H$_4$)	E_{bind}^{vdW} (eV/N$_2$H$_4$)	E_{cohe} (eV/N$_2$H$_4$)	E_{cohe}^{vdW} (eV/N$_2$H$_4$)	No. hydrogen bonds
2(A)	−1.12	−0.57	−1.14	−0.53	−0.02	−0.02	1
2(B)	−1.06	−0.50	−1.19	−0.54	0.06	−0.01	1
2(C)	−1.09	−0.45	−1.10	−0.51	−0.04	−0.03	1
3(A)	−1.10	−0.55	−1.10	−0.51	−0.04	−0.03	2
3(B)	−1.03	−0.56	−1.15	−0.53	0.06	−0.01	2
3(C)	−1.01	−0.59	−0.97	−0.52	−0.10	−0.04	2
4	−1.07	−0.57	−1.06	−0.52	−0.05	−0.04	3
5	−1.06	−0.57	−1.05	−0.52	−0.05	−0.04	4
6	−1.01	−0.52	−1.00	−0.48	−0.05	−0.04	4
9	−0.95	−0.58	−0.92	−0.52	−0.07	−0.05	6

Fig. 4. Top and side views of the charge density difference induced by deposition of 5 and 9 hydrazine molecules on Cu(111). The isosurface was set to ± 0.02 e Å^{-3}, where yellow and blue denote loss and gain of electron density respectively.

We also derived the topographical STM images, providing information about the spatial distribution of the valence band states in the vicinity of the Fermi energy (E_F), from the optimised structures of the different coverages composed of 5 and 9 hydrazine molecules. The positions of the atomic species adsorbed on a surface can be affected [3] in low temperature experimental STM, where they do not show the real space images of single molecules and small clusters on surfaces [37,38] for several reasons, such as high mobility of the molecules during adsorption resulting in immediate formation of larger clusters and error in cluster assignment. Moreover, tip interactions can perturb the image by vibrational excitation [39] or restructuring [40] and dissociating adsorbed molecules [41]. However, simulated STM images do not suffer from any external perturbations.

We have tested different potentials with respect to the Fermi level energy and concluded that a bias of −1.50 eV is enough to provide a clear STM image. Fig. 5 shows the STM images at a density of 8×10^{-5} e Å^{-3} and distance of 1.7 Å for the hydrazine assembly composed of 5 molecules and for full coverage with 9 molecules at a density of 2×10^{-4} e Å^{-3}, where the tip is at 1.4 Å from the highest atom. The insets in Fig. 5 clearly show the trans and gauche conformers that determine the STM images. As there is no experimental STM image to compare with, our simulated STM images for the hydrazine networks on Cu(111) are at the moment a good reference for future experiment.

The density of states (DOS) in Fig. 6 explains some features of the STM owing to its relationship to the partial charges. The negligible appearance of DOS of hydrogen atoms in the energy range [−1.5–0] eV explains why they are not observed at that bias in the STM images. The N atoms of the trans conformers show more and sharper peaks than the gauche structures in the energy range of [−1.5–0] eV, which explains why the protrusions from N atoms of trans conformers are more intensive in the STM image.

$$0.00008 \text{ eÅ}^{-3} \rightarrow 1.7 \text{ Å} \qquad 0.0002 \text{ eÅ}^{-3} \rightarrow 1.4 \text{ Å}$$
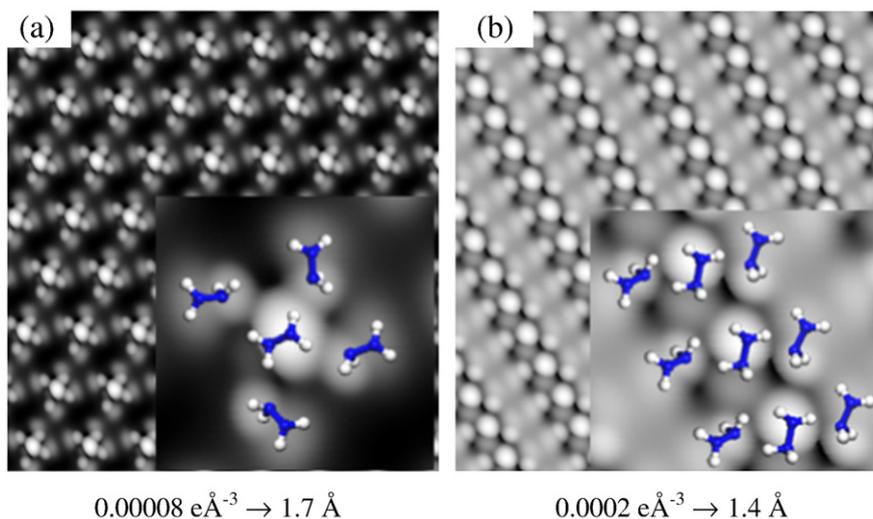
Fig. 5. Simulated STM images of the hydrazine network with a) 5 and b) 9 hydrazine molecules at a simulated bias of −1.5 V. Insets show enlargement of the STM images. Densities and tip distances are also indicated (N = blue, H = white).
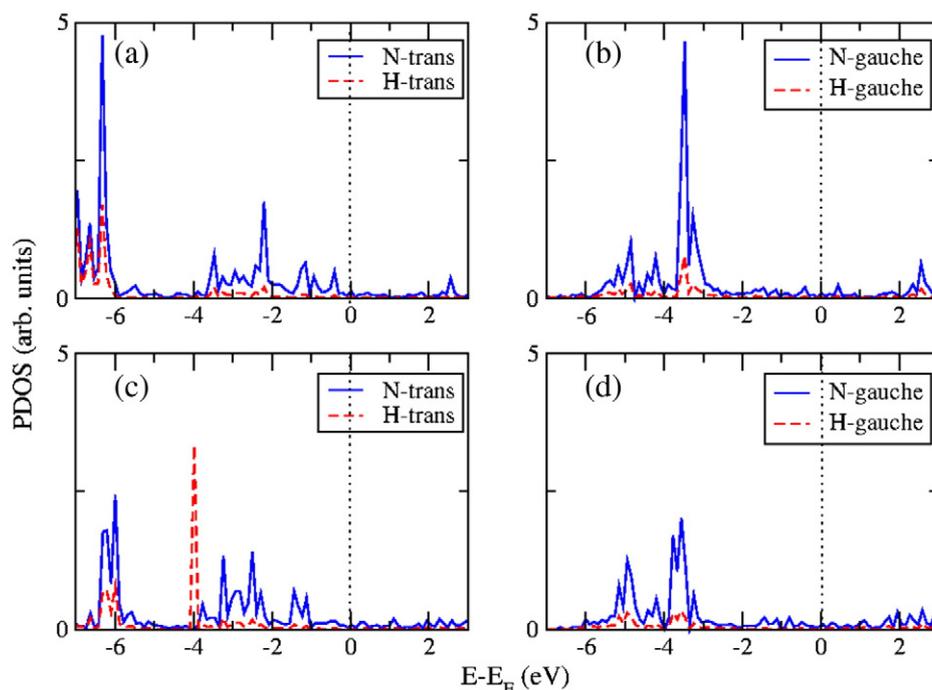
Fig. 6. The average PDOS of N and H atoms of trans and gauche conformations of N_2H_4 corresponding to $[N_2H_4]_5$ cluster in (a) and (b); and the full coverage $[N_2H_4]_9$ cluster in (c) and (d) on the Cu(111) surface. E = 0 eV corresponds to the Fermi level.

In order to clarify the effect of the hydrazine coverage on the binding and cohesion energies, we have analysed these energies for each structure in relation to the number of molecules in the assembled layer. A linear trend is presented in Fig. 7, indicating that while the cohesion energy remains almost constant with increasing number of molecules, the adsorption energy as well as the binding energy between the assembled hydrazine layer and the surface become less important. This trend confirms that the molecule–molecule interactions are weak and the hydrazine network is led by the binding energy, which contributes more to the adsorption energy than the cohesion energy.

The equilibrium morphology of a crystal is determined by the surface free energies. Wulff's Theorem [42] states that a polar plot of surface free energy versus the orientation of normal vectors would give the crystal morphology grown under thermodynamic equilibrium based on the approach of Gibbs, [43] who proposed that the equilibrium form of a crystal should possess minimal total surface free energy for a given volume. Lattice dynamics simulations have shown that the contribution of the excess entropy term to the surface free energy is small compared to the enthalpy term, as the differences between the entropies of the bulk and the surface are small. Hence, for solid surfaces the
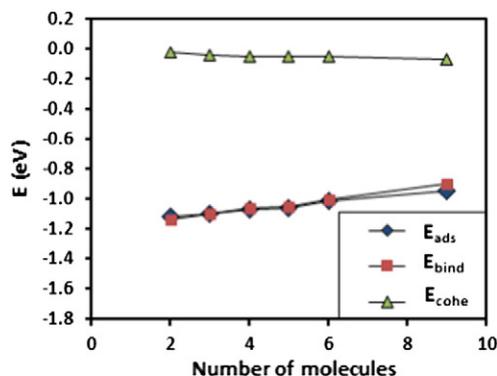
surface energy is a close approximation for the surface free energy [44] and the surface energies can therefore be assumed to determine the equilibrium morphology of the crystal.

The experimental study by Lisiecki [9] showed that controlling the hydrazine concentration is a key parameter enabling the size and shape control of copper nanoparticles. As the energy of the system changes linearly with respect to the hydrazine coverage, the hydrazine chemical potential remains constant and we have calculated the relaxed surface energy (γ) of the Cu(111) surface for the lowest-energy adsorption configurations at different hydrazine coverages. Fig. 8 shows the variation of the Cu(111) surface energy as a function of N_2H_4 coverage. As the increase in surface energy with hydrazine coverage is negligible, we may deduce that hydrazine does not affect the particles' morphology through the Cu(111), although it may of course have a more noticeable effect on surfaces with lower coordinations, which tend to be more reactive and whose surface energies tend to be more affected by adsorbates [45,46].

3.3. Temperature programmed desorption

In order to extrapolate the electronic structure results to real conditions we have simulated the temperature programmed desorption
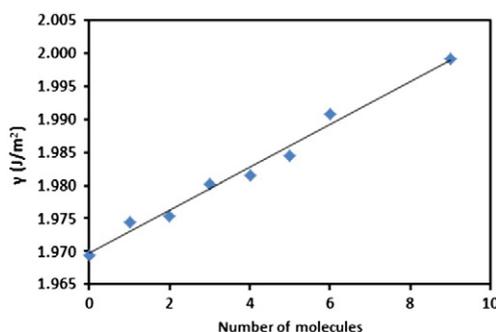

Fig. 7. Adsorption (E_{ads}), binding (E_{bind}) and cohesion (E_{cohe}) energies of the lowest-energy adsorption structures as a function of the number of hydrazine molecules.

Fig. 8. Surface energy (γ) of the Cu(111) surface for the lowest-energy adsorption structures as a function of the number of molecules. The linear trend-lines in the plots fit the equation y = 0.0034x + 1.9688, R^2 = 0.98.

(TPD) of N_2H_4 from the Cu(111) surface, considering pre-adsorbed N_2H_4 molecules with different coverages to mimic an experimental batch reactor with a high pumping speed to avoid re-adsorption of the molecule. The energy interaction is coverage dependent, as derived from our results for coverages between 0.06 and 0.25 ML N_2H_4 coverage, where a monolayer (ML) is defined as the number of molecules divided by the number of Cu atoms on the surface.

The N_2H_4 pressure and coverage as a function of time with the rate constant of k are derived from the following set of differential equations:

$$\frac{dP_{N_2H_4}}{dt} = k\theta_{N_2H_4} \tag{7}$$

$$\frac{d\theta_{N_2H_4}}{dt} = -k\theta_{N_2H_4} \tag{8}$$

where θ is the coverage in ML and t is the time.

In the heterogeneous catalytic system, the constant rate of desorption process is computed using the transition-state theory by Eyring [47] and Evans and Polanyi [48], as follows;

$$k = A_0 \exp\left(\frac{-E_a}{k_B T}\right) = \frac{k_B T}{h} \frac{q_{TS}}{q_{IS}} \exp\left(\frac{-E_a}{k_B T}\right) \tag{9}$$

where h is the Plank constant, k_B is the Boltzmann constant, T is the temperature, A_0 is the pre-exponential factor, E_a is the binding energy and q_{IS} and q_{TS} are the partition functions of reactants and transition states, respectively. The partition function q_{IS} includes all the vibrational modes, while q_{TS} is the partition function for the transition state, where the only degree of freedom the molecule has is vibrational, from which the vibration between the molecule and the surface representing the reaction coordinate has been excluded. The values of the N_2H_4 desorption rate constant and pre-exponential factor at 150 and 300 K are reported in Table 4.

Fig. 9 shows the simulated TPD spectra of molecular N_2H_4 on the Cu(111) surface, where the derivative of the N_2H_4 partial pressure with respect to the temperature results in a peak showing the temperature at which the N_2H_4 pressure reaches its maximum. Since experimental reports show that hydrazine starts to decompose at around 300 K [49], we have considered a temperature range between 100 and 300 K to investigate N_2H_4 desorption, without involving hydrazine reactions on the Cu surface. A heating rate of 1 K/min was applied, measuring the pressure every second. From Fig. 9 it is clear that N_2H_4 desorption takes place between 150 and 200 K from the Cu(111) surface. Similar desorption temperatures have been reported for hydrazine on rhodium [50] and Ir_n/Al_2O_3 [51] surfaces.

4. Conclusions

We have presented a theoretical study using DFT-D2 of the assembly of hydrazine networks adsorbed on the Cu(111) surface. Our results show that the molecule–molecule interactions are very weak and arise mostly from dispersive forces. We conclude that binding of the N_2H_4 molecules with the Cu surface, plus dispersive forces between adsorbate and surface are the main interactions driving the assembled adsorbate networks, although the cohesion energies between the molecules, arising primarily from long-range interactions, also affect
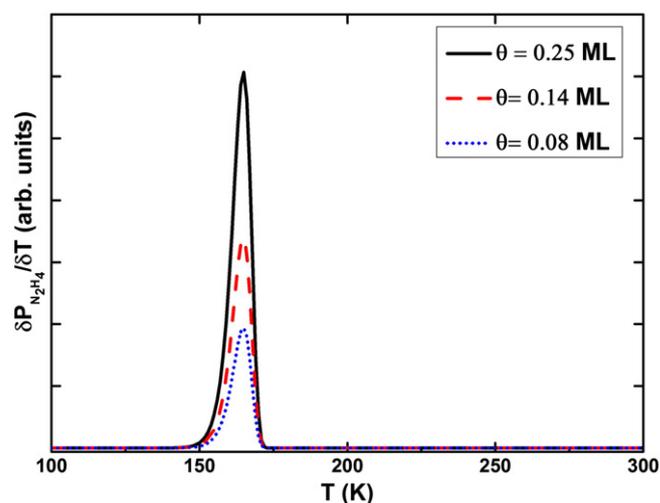

Fig. 9. Simulated TPD curves for N_2H_4 desorption from Cu(111) surface for a reaction time of 1 s and heating rate of 1 K/min at different initial coverages.

the arrangement of the molecules in the surface overlayer. The relatively large dispersion contributions to the cohesion energies indicate that the molecule–molecule interactions arise mostly from vdW forces and that hydrogen-bonding is the smallest contributory factor in the hydrazine assembly. Our charge density difference calculations show that the molecule and substrate share electrons, while no charge transfer was observed between molecules. The STM images for the two hydrazine networks composed of five and nine molecules were calculated, where the observed protrusions arise from the trans conformers. We have also investigated the surface energy as a function of hydrazine concentration, indicating that variation in the hydrazine coverage on the Cu(111) should not affect significantly the shapes of the copper nanoparticles, and further investigation of other Cu facets of the nanoparticles is therefore required to obtain the effect of hydrazine coverage on their surface energies. Temperature programmed desorption of hydrazine from the Cu(111) surface was simulated for different hydrazine coverages, showing a desorption peak between 150 and 200 K.

Appendix A. Supplementary data

Supplementary data to this article can be found online at http://dx.doi.org/10.1016/j.susc.2015.04.001.

Table 4
Calculated pre-exponential factors (A_0) and desorption rate constants (k) for N_2H_4 from Cu(111) at 150 and 300 K are reported.

	A_0 (s^{-1})		k (s^{-1})	
	150 K	300 K	150 K	300 K
N_2H_4 (ads) → N_2H_4 (g)	8.39×10^{11}	2.31×10^{11}	4.14×10^{-5}	5.68×10^{7}

References

[1] K.S. Mali, J. Adisoejoso, E. Ghijsens, I. De Cat, S. De Feyter, Acc. Chem. Res. 45 (2012) 1309.
[2] K.S. Thanthiriwatte, E.G. Hohenstein, L.A. Burns, C.D. Sherrill, J. Chem. Theory Comput. 7 (2011) 88.
[3] S. Irrera, A. Roldan, G. Portalone, N.H. De Leeuw, J. Phys. Chem. C 117 (2013) 3949.

[4] Y.S. Kim, J.Y. Koo, H. Kim, Phys. Rev. Lett. 101 (2008) 256105.
[5] A. Kuhnle, Curr. Opin. Colloid Interface Sci. 14 (2009) 157.
[6] M. Mura, A. Gulans, T. Thonhauser, L. Kantorovich, Phys. Chem. Chem. Phys. 12 (2010) 4759.
[7] M. Smerieri, L. Vattuone, D. Costa, F. Tielens, L. Savio, Langmuir 26 (2010) 7208.
[8] I. Tranca, M. Smerieri, L. Savio, L. Vattuone, D. Costa, F. Tielens, Langmuir 29 (2013) 7876.
[9] I. Lisiecki, J. Phys. Chem. B 109 (2005) 12231.
[10] A. Filankembo, S. Giorgio, I. Lisiecki, M.P. Pileni, J. Phys. Chem. B 107 (2003) 7492.
[11] C.L. Kitchens, M.C. McLeod, C.B. Roberts, J. Phys. Chem. B 107 (2003) 11331.
[12] I. Lisiecki, M.P. Pileni, J. Am. Chem. Soc. 115 (1993) 3887.
[13] C. Salzemann, L. Lisiecki, J. Urban, M.P. Pileni, Langmuir 20 (2004) 11772.
[14] J. Tanori, M.P. Pileni, Adv. Mater. 7 (1995) 862.
[15] J. Tanori, M.P. Pileni, Langmuir 13 (1997) 639.
[16] G. Kresse, J. Furthmuller, Phys. Rev. B 54 (1996) 11169.
[17] G. Kresse, J. Furthmuller, Nato. Sc. S. Ss. III C. S. 6 (1996) 15.
[18] G. Kresse, J. Hafner, Phys. Rev. B 47 (1993) 558.
[19] G. Kresse, J. Hafner, Phys. Rev. B 49 (1994) 14251.
[20] J.P. Perdew, K. Burke, M. Ernzerhof, Phys. Rev. Lett. 77 (1996) 3865.
[21] G. Kresse, D. Joubert, Phys. Rev. B 59 (1999) 1758.
[22] P.E. Blochl, Phys. Rev. B 50 (1994) 17953.
[23] S. Grimme, J. Comput. Chem. 27 (2006) 1787.
[24] S. Grimme, J. Comput. Chem. 25 (2004) 1463.
[25] S.S. Tafreshi, A. Roldan, N.Y. Dzade, N.H. de Leeuw, Surf. Sci. 622 (2014) 1.
[26] S.S. Tafreshi, A. Roldan, N.H. de Leeuw, J. Phys. Chem. C 118 (2014) 26103.
[27] N.Y. Dzade, A. Roldan, N.H. de Leeuw, J. Chem. Phys. 139 (2013).
[28] H.J. Monkhorst, J.D. Pack, Phys. Rev. B 13 (1976) 5188.
[29] H. Wawra, Z. Metallkd. 66 (1975) 492.
[30] S.Å. Lindgren, L. Walldén, J. Rundgren, P. Westrin, Phys. Rev. B 29 (1984) 576.
[31] S.P. Tear, K. Roll, M. Prutton, J. Phys. C Solid State 14 (1981) 3297.
[32] R.F.W. Bader, Atoms in Molecules: A Quantum Theory, Clarendon Press, Oxford, 1990.
[33] G. Henkelman, A. Arnaldsson, H. Jonsson, Nato. Sc. S. Ss. III C. S. 36 (2006) 354.
[34] J. Tersoff, D.R. Hamann, Phys. Rev. B 31 (1985) 805.
[35] D.E.P. Vanpoucke, G. Brocks, Phys. Rev. B 77 (2008) 241308.
[36] T.D. Daff, N.H. de Leeuw, J. Mater. Chem. 22 (2012) 23210.
[37] A. Hodgson, S. Haq, Surf. Sci. Rep. 64 (2009) 381.
[38] M.A. Henderson, Surf. Sci. Rep. 46 (2002) 1.
[39] H. Gawronski, K. Morgenstern, K.H. Rieder, Eur. Phys. J. D 35 (2005) 349.
[40] H. Gawronski, J. Carrasco, A. Michaelides, K. Morgenstern, Phys. Rev. Lett. 101 (2008) 136102.
[41] K. Morgenstern, K.H. Rieder, Chem. Phys. Lett. 358 (2002) 250.
[42] G. Wulff, Z. Kristallogr. Mineral 34 (1901) 449.
[43] J.W. Gibbs, In Collected Works, Longman, New York, 1928.
[44] D. Mkhonto, N.H. de Leeuw, J. Mater. Chem. 12 (2002) 2633.
[45] T.D. Daff, D. Costa, I. Lisiecki, N.H. de Leeuw, J. Phys. Chem. C 113 (2009) 15714.
[46] T.D. Daff, N.H. de Leeuw, Chem. Mater. 23 (2011) 2718.
[47] H. Eyring, J. Chem. Phys. 3 (1935) 107.
[48] M.G. Evans, M. Polanyi, Trans. Faraday Soc. 31 (1935) 0875.
[49] Y.K. Alhaydari, J.M. Saleh, M.H. Matloob, J. Phys. Chem.-Us 89 (1985) 3286.
[50] J. Prasad, J.L. Gland, Langmuir 7 (1991) 722.
[51] S. Lee, C.Y. Fan, T.P. Wu, S.L. Anderson, J. Phys. Chem. B 109 (2005) 381.